

HIGH-MASS STAR FORMATION THROUGH FAR-INFRARED STUDIES

R. P. Verma, S. K. Ghosh, and T. N. Rengarajan¹

TIFR, Mumbai, India

RESUMEN

Se han observado el complejo de formación de estrellas de alta masa RCW 106, dos regiones H II compactas y un grumo de CO en el infrarrojo lejano (a ~ 150 y $210 \mu\text{m}$) utilizando el telescopio de 1 m llevado por un globo de TIFR. Se obtuvieron mapas de intensidad, la temperatura del polvo y la profundidad óptica con una resolución de $\sim 1'.3$. Utilizando 23 fuentes en el complejo RCW 106, se encontró que la pendiente de la función inicial de masa es -1.73 ± 0.5 . A partir de observaciones hechas con el satélite *ISO*, se obtuvieron flujos en las bandas de los PAH para 3 fuentes compactas. Se ha modelado las distribuciones de energía espectral por medio de cálculos de transporte radiativo.

ABSTRACT

RCW 106, a high-mass star-forming complex, two compact H II regions and a CO clump have been observed in the far infrared (at ~ 150 and $210 \mu\text{m}$) using the TIFR 1 m balloon-borne telescope. Maps of intensity, dust temperature and optical depth with $\sim 1'.3$ resolution were obtained. Using 23 sources in the RCW 106 complex, the slope of the IMF is found to be -1.73 ± 0.5 . From *ISO* observations, fluxes in the PAH bands have been obtained for the 3 compact sources. Radiation transfer calculations have been performed for modeling the spectral energy distributions.

Key Words: **H II REGIONS — INFRARED: ISM — ISM: INDIVIDUAL (RCW 106, IRAS 19181+1349, IRAS 20178+4046, IRAS 20286+4105) — STARS: FORMATION**

1. INTRODUCTION

Far-infrared (FIR) observations are important for the study of high-mass star formation (HMSF) since most of the luminosity of the embedded sources is radiated at these wavelengths. The TIFR group has been studying HMSF using a 1 m balloon-borne telescope. In this paper, we present the results of observations of RCW 106, a large southern star-forming complex, two ultracompact H II (UCH) regions, and a compact CO clump. We make use of the presence of a large number of embedded high mass stars in RCW 106 to obtain the slope of the IMF at a very young age. For the compact sources *Infrared Space Observatory* (*ISO*) observations have also been undertaken both to get the spectral energy distributions (SEDs) in the mid-IR and the fluxes in the PAH bands. The samples also provide us an opportunity to understand the physical conditions of the envelopes of the sources through radiation transfer modeling of the SEDs.

2. OBSERVATIONS

The sources discussed in this paper were observed using the TIFR 1 m balloon-borne telescope flown

on 1994 February 20 from Hyderabad, India. The details of the telescope and the observational procedures have been described by Ghosh et al. (1988). The photometer used had two arrays each consisting of six ³He-cooled bolometers. The field of view of each detector was $1'.6$. The two arrays viewed the same sky simultaneously in bands centered around 150 and $210 \mu\text{m}$, respectively. The details of the photometer and the flux calibration procedure have been described by Verma, Rengarajan, & Ghosh (1993), Ghosh et al. (2000), and Karnik et al. (2001). The mapping was done by raster scans and the intensity maps were generated through a deconvolution procedure based on the maximum entropy method with a resolution of $\sim 1'.3$. IRAS 19181+1349, 20178+4046, and 20286+4105 were also observed with ISOCAM on board *ISO*. Images were obtained in filters centered at 3.3, 3.72, 6.0, 6.75, 7.75, 9.62, and $11.4 \mu\text{m}$ covering four PAH bands and the neighboring continuum. *IRAS* HIRES maps at 12, 25, 60, and $100 \mu\text{m}$ were also generated for all the sources.

3. RESULTS AND DISCUSSION

3.1. RCW 106

Figure 1 shows the intensity maps of RCW 106 at 150 and $210 \mu\text{m}$. In addition to seeing the *IRAS*

¹INAOE, Mexico.

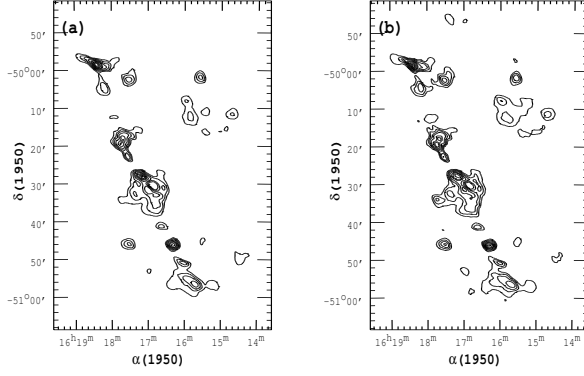


Fig. 1. Intensity maps of RCW 106 at (a) $150 \mu\text{m}$ and (b) $210 \mu\text{m}$. Contour levels drawn are at 1, 2.5, 5, 10, 20, 30, 50, 70, and 90 percent of the peak intensities of 9728 and 4375 Jy arcmin^{-2} respectively.

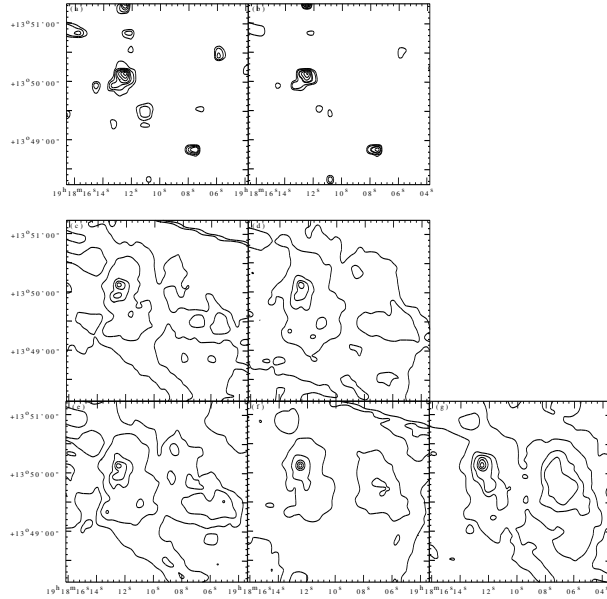


Fig. 2. The ISOCAM maps of the region around IRAS 19181+1349 at (a) $3.30 \mu\text{m}$, (b) $3.72 \mu\text{m}$, (c) $6.00 \mu\text{m}$, (d) $6.75 \mu\text{m}$, (e) $7.75 \mu\text{m}$, (f) $9.62 \mu\text{m}$, and (g) $11.4 \mu\text{m}$. The contour levels are at 0.9, 0.7, 0.5, 0.3, 0.2, 0.1, and 0.05 times the peak intensities which in the order of wavelength are 19.5, 17.8, 36.5, 37.7, 70.2, 37.8, and $58.7 \text{ Jy arcmin}^{-2}$.

sources in the region, we observe additional resolved sources giving a total of 23. For 10 sources we also have associations with radio continuum sources (Shaver & Goss 1970; Retallack & Goss 1980). We have also generated the maps of dust temperature and optical depth using our flux ratios and assuming an emissivity $\propto \lambda^{-2}$. The temperature map shows evidence for the presence of blister sources. For the 23 sources detected we can estimate the luminosity

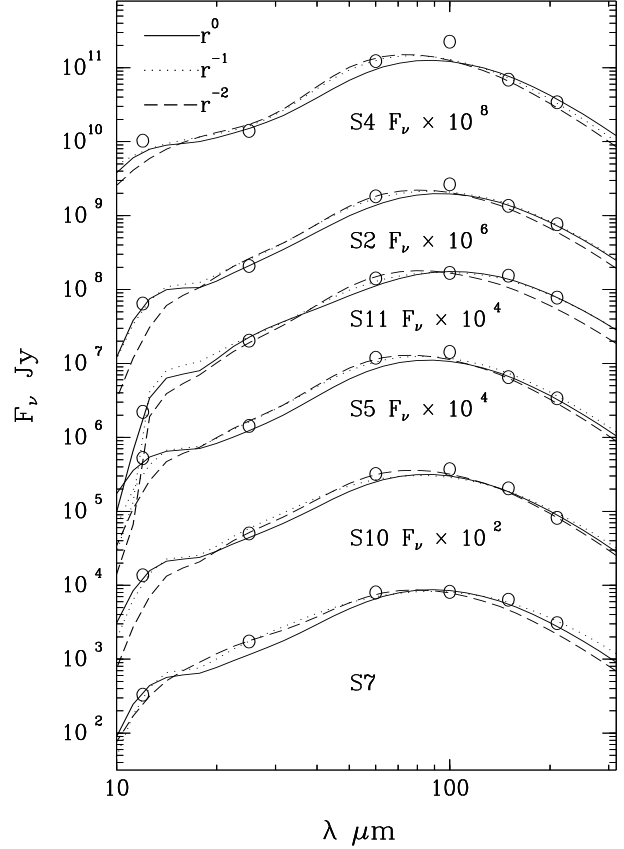


Fig. 3. Spectral energy distribution of 6 sources in the RCW 106 complex. The lines shown are fits from radiation transfer models. The different lines depict fits for three different power-law exponents of the radial density distribution. Note that for the sake of clarity the flux densities have been multiplied by different constant factors for 5 sources.

taking a distance of 3.6 kpc, and hence the mass, assuming the embedded stars to be ZAMS. From this, the exponent of the initial mass function $\xi(\log m)$ is found to be -1.73 ± 0.5 , similar to that for cluster stars. Note that the IMF slope has been determined only for very few young ($< 0.1 \text{ Myr}$) complexes.

3.2. Compact Sources

The maps of the 3 compact sources show several resolved sources. For lack of space we do not discuss the details. As an example, we show in Figure 2 the ISOCAM maps of IRAS 19181+1349 wherein one can see several resolved sources. In the long wavelength *ISO* maps two groups of sources separated by $1/5$ are seen. These two components are also seen in our $210 \mu\text{m}$ map, but not in the *IRAS* 60 and $100 \mu\text{m}$ maps. From the *ISO* maps we derive the PAH fluxes in the 3.3, 6.2, 7.7, and $11.4 \mu\text{m}$ bands. The $7.7 \mu\text{m}$ feature is found to be the strongest while

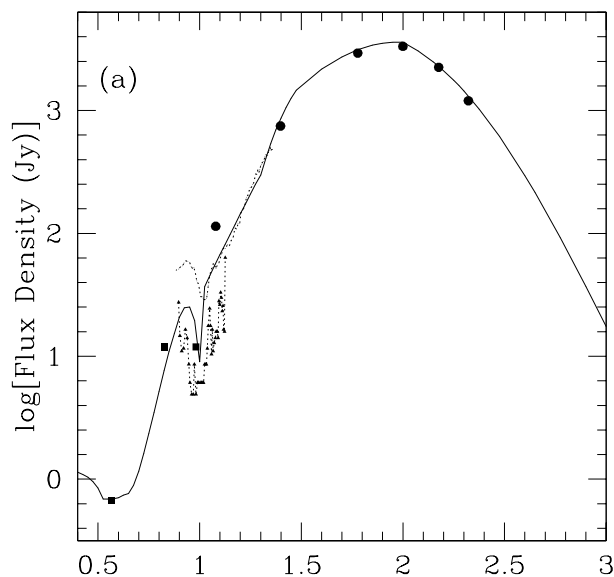


Fig. 4. The flux density vs $\log \lambda (\mu\text{m})$ of IRAS 20178+4046. The symbols are: circles—this paper and *IRAS* HIREs; squares—ISOCAM; triangles—ground based measurements of Faison et al. (1998); dotted line—*IRAS* LRS. The solid line is the model fit for density exponent = 2.

the $6.2 \mu\text{m}$ feature is mostly absent. Further, we find that the band ratios except those involving the $6.2 \mu\text{m}$ feature agree with other measurements for compact H II regions, but they seem to be different from the values for general H II regions. The spatial distribution of PAH emission is found to be diffuse and widespread. We have computed the mean and standard deviation of flux ratios using the values on pixel by pixel basis. The $11.3 \mu\text{m}$ to $7.7 \mu\text{m}$ ratios (mean \pm rms) are found to be 0.3 ± 0.39 , 0.84 ± 0.4 and 1.07 ± 0.64 for IRAS 19181+1349, 20178+4046, and 20286+4105, respectively, while the $7.7 \mu\text{m}$ to $3.3 \mu\text{m}$ flux ratios are 23.2 ± 11.8 , 19.9 ± 14.0 , and 13.4 ± 11.7 , respectively. The scatter in the values of the ratios in each source is real and represents genuine spatial variation. The difference between the mean ratio for IRAS 19181+1349 and the other two sources is perhaps an indication of their evolutionary stages.

3.3. Radiation Transfer Calculation

The emergent SED of an embedded source depends on the physical parameters of the envelope and

these can be deduced by fitting the SED to model radiation transfer calculations. We have performed this for 13 sources in RCW 106 and the 3 compact sources. The details of the calculation procedure have been given by Mookerjea et al. (1999). Here, we will discuss only the radial density dependence represented as $\rho(r) \propto r^{-n}$. An example of model fits for 6 sources in RCW 106 is shown in Figure 3. For most sources the best fit is obtained for $n = 0$ or 1, different from the value of 1.5 to 2 expected on the basis of collapse models (Shu, Adams, & Lizano 1987). However, we do find that the best fit (shown in Figure 4) for IRAS 20178+4046 is for $n = 2$. For the 3 compact sources we have also computed the source size as a function of wavelength for the best fit models and these agree with observations.

4. SUMMARY

Far-infrared observations of RCW 106 have been presented. Twenty three sources are resolved in this complex and the slope of the IMF is found to be -1.73 ± 0.5 . Three compact sources (UCH and CO clump) have been observed in the far- and mid-IR. Fluxes in the PAH bands have been determined. For these 3 sources and 13 in RCW 106, radiation transfer calculations have been done to understand the properties of the envelopes.

REFERENCES

- Faison, M., Churchwell, E., Hofner, P., Hackwell, J., Lynch, D. K., & Russel, R. W. 1998, *ApJ*, 500, 280
 Ghosh, S. K., Iyengar, K. V. K., Rengarajan, T. N., Tandon, S. N., Verma, R. P., & Daniel, R. R. 1988, *ApJ*, 330, 928
 Ghosh, S. K., Mookerjea, B., Rengarajan, T. N., Tandon, S. N., & Verma, R. P. 2000, *A&A*, 363, 744
 Karnik, A. D., Ghosh, S. K., Rengarajan, T. N., & Verma, R. P. 2001, *MNRAS*, 326, 293
 Mookerjea, B., Ghosh, S. K., Karnik, A. D., Rengarajan, T. N., Tandon, S. N., & Verma, R. P. 1999, *ApJ*, 522, 285
 Retallack, D. S., & Goss, W. M. 1980, *MNRAS*, 193, 261
 Shaver, P. A., & Goss, W. M. 1970, *Aust. J. Phys. Suppl.*, 14, 133
 Shu, F. H., Adams, F. C., & Lizano, S. 1987, *ARA&A*, 25, 23
 Verma, R. P., Rengarajan, T. N., & Ghosh, S. K. 1993, *Bull. Astr. Soc. India*, 21, 489

S. K. Ghosh and R. P. Verma: Tata Institute of Fundamental Reserach, Homi Bhabha Road, Mumbai (Bombay), India (swarna, vermarp@tifr.res.in).

T. N. Rengarajan: Instituto Nacional de Astrofisica Óptica y Electrónica, Tonantzintla, Puebla 72840, Mexico (renga@inaoep.mx).